

QUANTITATIVE ANALYSIS OF FOLDS BY MEANS OF ORTHORECTIFIED PHOTOGRAMMETRIC 3D MODELS: A CASE STUDY FROM MT. CATRIA, NORTHERN APENNINES, ITALY

AMERIGO CORRADETTI (amerigo.corradetti@unina.it)

STEFANO TAVANI (stefano.tavani@unina.it)

MARIO RUSSO (hysteria.mr@gmail.com)

DiSTAR, Università di Napoli Federico II, Naples, Italy

PAU CAZO ARBUÉS (pau.arbues@ub.edu)

PABLO GRANADO (pablomartinez_granado@ub.edu)

Institut de Recerca Geomodels, Universitat de Barcelona, Barcelona, Spain

Abstract

A 3D model of a plunging meso-scale chevron fold affecting Mesozoic limestone has been generated, scaled and oriented applying a photogrammetrically based workflow. Bedding measurements allowed extracting the statistical direction of intersection between the bedding planes (the fold's β axis), allowing for the orthorectification of the 3D model and the construction of a photo-realistic cross section. The methodology in this contribution constitutes an innovative tool, available to all, for the accurate quantitative analysis of geological structures.

KEYWORDS: chevron fold, data analysis, digital photogrammetry, geological outcrop, 3D model

INTRODUCTION

PHOTOGRAMMETRIC IMAGE-BASED 3D MODELLING is considered as a fast, economically affordable and trustworthy alternative to lidar (light detection and ranging) for the 3D digital representation of geological outcrops (James and Robson, 2012). The user-friendly nature of this rapidly improving technique is, in fact, allowing a large community of geoscientists to construct detailed digital models of geological exposures (for example, Pringle et al., 2001; Sturzenegger and Stead, 2009; Bistacchi et al., 2011; 2015; Favalli et al., 2012; Massironi et al., 2013; Tavani et al., 2014; Reitman et al., 2015; Thiele et al., 2015; Vollgger and Cruden, 2016). More specifically, the application of this technique is becoming widely accepted in dealing with the characterisation of geological structures and related structural elements (fractures and folds) from digital outcrop data (for example, McCaffrey et al., 2008; Pearce et al., 2011; Bemis et al., 2014; Vasuki et al., 2014; Seers and Hodgetts, 2016a; Vollgger and Cruden, 2016; Corradetti et al., 2017). The photogrammetric method

(Remondino and El-Hakim, 2006) is an estimative technique through which the metric data of a 3D object (shape, position and size) are obtained by estimating the spatial coordinates of each point in the photographs. Since each photograph contains only 2D coordinates, at least two overlapping images taken from different points of view are needed to estimate the 3D coordinates of points. This task can be handled by structure-from-motion (SfM) algorithms (Ullman, 1979), which have developed strongly over the past two decades. For instance, recent advances have been made with respect to image-matching techniques (Gruen, 2012), which are methods developed to establish the relationship between different images (with different point of view, focal distance, lighting conditions and so on). One example is the scale-invariant feature transform (SIFT) algorithm (Lowe, 2004), developed to transform image data into scale-invariant coordinates relative to local features. Matching algorithms are very sensitive to angular deviation between overlapping images; reconstruction accuracy improves as this angle increases up to a certain point, after which matching will be prevented due to the component image pairs being too dissimilar (Moreels and Perona, 2007; Bemis et al., 2014; James and Robson, 2014). Once a model is generated, spatial referencing by means of control points is needed to improve accuracy and to scale and orient the model (normally using a bundle adjustment) before any data or spatial consideration is derived from the real outcrop. This control-point task is commonly solved using extremely accurate tools. These are often total stations, having an accuracy of a few millimetres per kilometre and about 2" for angular measurements (Feng et al., 2001). Note that laser scanners (Hodgetts, 2013) are, unfortunately, still quite heavy, bulky and, ultimately, less affordable (although they are an accurate alternative to photogrammetry for generating the 3D model).

AIM OF THE WORK

In this study, to meet the needs of many field geologists and geoscientists (especially those working in remote areas) interested in 3D modelling of outcrops, scaling and orientation of a 3D model was addressed using lightweight and easily accessible tools (Rieke-Zapp et al., 2009; Tavani et al., 2016). Scaled and oriented 3D models can be used for several purposes. One of them is particularly useful to field geologists, and consists of the possibility of visualising the 3D digital model in an orthographic projection mode. This can be achieved by using geologically relevant directions of view, such as the fold axis or fracture–bedding intersection (Tavani et al., 2016). For instance, it is well known amongst geologists that the profiles of folded areas can be significantly misinterpreted in terms of bed thickness and orientation due to perspective distortion (apparent geometry) caused by the intersection between the geological structure and the topography. This distortion can be particularly significant in rugged mountainous regions. In the past, such a problem has been tackled by time-consuming geometrical techniques using geological maps, bedding orientation and fold-axis plunge data. A classic example is the reconstruction of the Dent de Morcles Nappe in south-west Switzerland by Ramsay and Huber (1987). The procedure of outcrop “orthorectification” (Vasuki et al., 2014; Tavani et al., 2016), for instance, allows the production of photo-realistic cross sections of geological structures showing the real geometry of structures. Digital orthorectification along proper directions allowed the authors to take measurements that were not easy to gather in the field. By means of 3D models it is therefore possible to switch from a strictly qualitative to quantitative analysis of outcrops and geological structures. The method might be applied to overcome several technical limitations that are generally encountered during fieldwork including perspective distortion, outcrop inaccessibility or the lack of instruments for quantitative acquisition of data.

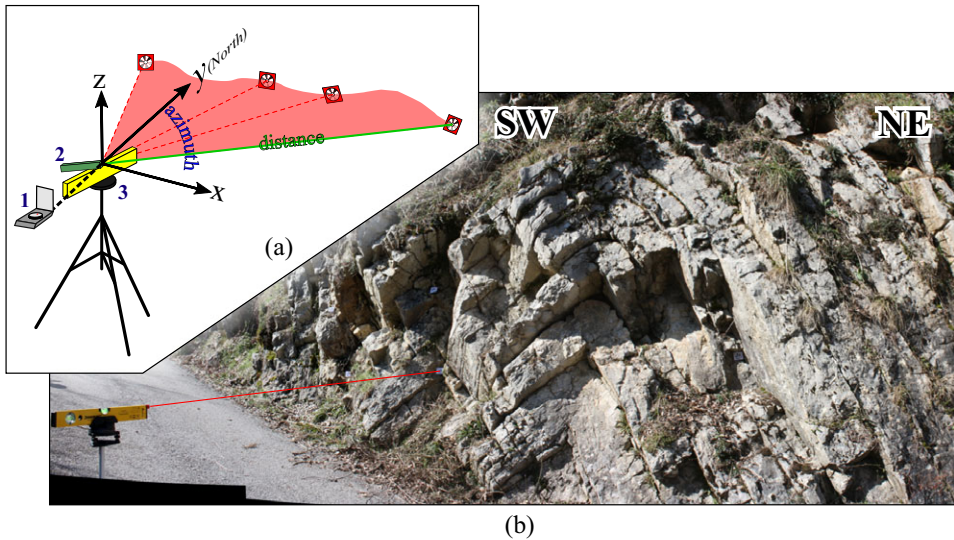


FIG. 1. (a) Scheme showing the method adopted to calculate the coordinates of the target “sticks” to the outcrop at the same elevation as the laser level. The elevation of these targets is at 0 metres since the laser level is assigned (X, Y, Z) coordinates of $(0, 0, 0)$. The X and Y coordinates are calculated by simple trigonometry using the distance achieved using a laser rangefinder and the azimuth derived from the graduated dial of the laser level. Additional targets over the outcrop surface are placed to estimate errors in the model as explained in the text. (b) Photograph of the studied outcrop showing the laser level (left) in its working position with the red line indicating the positioning of one of the target sticks relative to the laser beam.

A case study from a plunging anticline (Fig. 1(b)) belonging to the Mt. Catria area of the northern Apennines, Italy has been reported. The folded layers studied display significant bed-thickness variations between the limbs of the fold and its hinge that could only be qualitatively estimated in the field. An orthorectified section oriented perpendicular to the axis of the anticline has been produced, allowing quantitatively describing and constraining the observed thickening and thinning relationships of the folded layers.

WORKFLOW

The general steps followed to produce a photo-realistic cross section of the outcrop is described here. The quality of image-based 3D models cannot be determined without knowing the position of points on the outcrop. Accurate positioning of points should be obtained, for instance by means of a total station, which is an expensive and heavy device. Nevertheless, extremely accurate positioning of points may be unnecessary for several applications in geology, especially when the size of the geological features that are collected from the model are orders of magnitude larger than the model accuracy. For instance, in optimal conditions (strongly coplanar but non-collinear points) the attitudes of bedding planes several tens-of-centimetres long can potentially be extracted from models having an accuracy lower than a centimetre without incurring errors larger than those achieved by measuring the bedding attitudes in the field with a compass. Furthermore, accurate models can be obtained even with consumer-grade digital cameras through the collection of oblique imagery that can significantly reduce systematic errors (Wackrow and Chandler, 2011; James and Robson, 2014).

In the field, a compass was used to orient the graduated dial (an azimuth precision of 1° is indicated by the manufacturer) that represents the origin of the selected local reference system (Fig. 1(a)). Using a laser level mounted on a graduated dial, four coded targets were positioned on the outcrop surface at zero-metre elevation (with a vertical precision of 0.29°). The position of these targets with respect to the origin (namely, the laser level) was recorded: the angular coordinates were obtained from the graduated dial; the distances were obtained using the laser distance meter (which constitutes a further target at the origin). A similar registration scheme, by means of accurate tools, was also used by Seers and Hodgetts (2013) to obtain key points for a rigid transformation for terrestrial lidar-derived point clouds; in a similar fashion, Seers and Hodgetts (2016a) obtained a similarity transformation for tetrahedral meshes derived using SfM multiview stereo (MVS). Four additional targets were placed randomly on the outcrop surface and only their distance from the origin was measured.

The outcrop was then extensively photographed from different positions providing a good overlap between each successive image (Fig. 2), including photographs oblique to the outcrop (Wackrow and Chandler, 2011). A set of photographs of the outcrop and the laser level (Fig. 1(b)) were included. By doing so, the laser level is used as the origin of the local coordinate system, and at least one control point is not collinear with the other targets at the zero elevation. This avoids possible rotation of the model around the line of intersection of the control points.

The model of the outcrop was built in PhotoScan (Plets et al., 2012; Bemis et al., 2014). After importing all photographs into this software, the targets were manually identified in each image and their positions included before the software estimated the position of the photographs. The distances from the origin to all targets in the 3D digital model were compared to the distances measured on the outcrop. This procedure was used as a proxy to assess whether major errors resulted from the construction of the model.

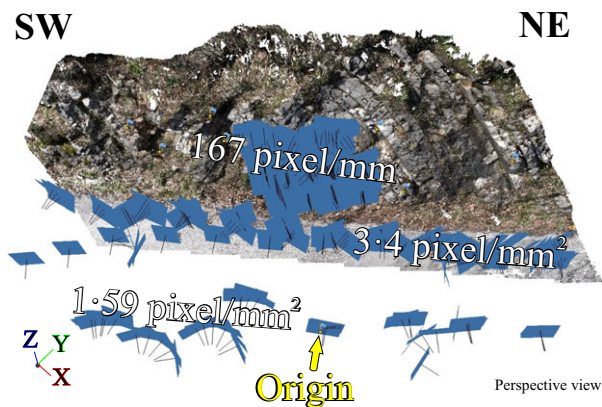


FIG. 2. Perspective view of the model showing the position of the photographs (blue) and location of the laser level (the origin). X, Y and Z axes' orientation refers to the software's internal coordinate system. The photographs' resolution indicated is calculated and averaged for those photographs taken perpendicularly to the outcrop (photographs not perpendicular to the outcrop have a lower resolution than indicated at a comparable distance).

The subsequent step was the extraction of geological data, such as bedding and fracture attitudes. This procedure was carried out on the textured mesh after importing it into the OpenPlot software (Tavani et al., 2011, 2014). The extracted data were then used to calculate the direction of interest to orthorectify the 3D model, thus producing the cross section of the outcrop. PhotoScan can only produce orthomosaics of certain predefined projection planes (namely, planes intersecting reference axes). For this reason, to generate a cross section of the outcrop, the model in PhotoScan was rotated applying a change of base so as to align the reference axis to the direction of interest. The rotation was carried out by recalculating the X , Y , Z coordinates of the targets through elementary transformation matrices.

CASE STUDY

Geological Setting

The outcrop for this case study is located in the Umbria–Marche outer sector of the northern Apennines (geologically analysed by, for example, Barchi et al., 1991). There, the Apennines are characterised by typical arcuate shape with north-eastern vergence (Barchi et al., 2001; Mazzoli et al., 2002), and by the presence of several anticlines (Marchegiani et al., 1999; Pierantoni et al., 2013; Beaudoin et al., 2016) involving a Mesozoic–Tertiary sedimentary succession. This study was focused on a meso-scale fold located in the frontal domain of the Mt. Catria anticline (Fig. 3). The Mt. Catria anticline is a NW–SE striking structure that was involved in the Apennines' Thrust Wedge during the Messinian (Elter et al., 1975; Bigi et al., 1989).

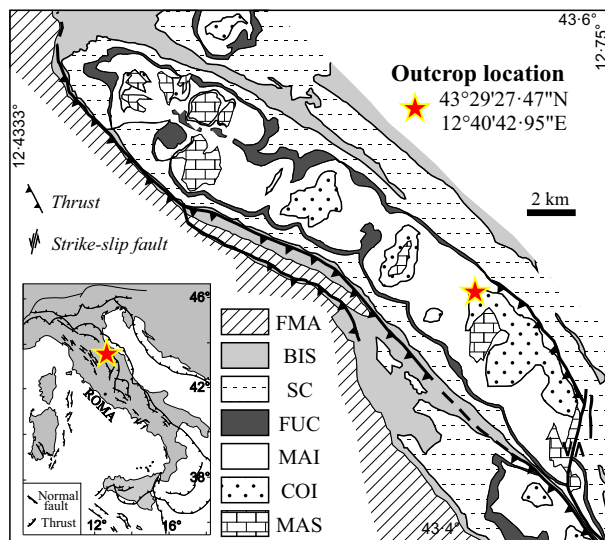


FIG. 3. In this figure a geological map of the Monte Catria anticline with its outcrop location is shown. Ages of the formations in the legend are: FMA, Marnoso-Arenacea Fm (Langhian – Serravallian); BIS, Scaglia Cinerea, Bisciaro and Schlier Fms (Priabonian – Tortonian); SC, Scaglie Fms (Cenomanian – Priabonian); FUC, Marne a Fucoidi Fm (Aptian – Cenomanian); MAI, Maiolica Fm (Tithonian – Aptian); COI, Corniola, Bosso and Calcare Diasprigni Fms (Sinemurian – Tithonian); MAS, Calcare Massiccio Fm (Hettangian – Sinemurian).

The case study outcrop is located near the town of Frontone, and consists of a WNW-plunging meso-scale anticline with narrow hinge and straight limbs (in other words a chevron fold) (Fig. 1(b)). The anticline affects Mesozoic strata of the Corniola Formation. This unit is constituted by greyish thin-to-medium bedded micritic limestones with nodules and layers of chert. The fold studied is characterised by both bedding-parallel and bedding-perpendicular pressure solution surfaces (PSS), as well as bedding-perpendicular joints and veins. Veins are particularly evident within the outer arc of the hinge zone, whereas the inner arc is affected by small-scale reverse faults (displacements of the order of a millimetre to a centimetre) and PSS, which contribute to produce the thickening of layers in the hinge zone.

Bedding, vein and fracture (that is, joints and stylolites) data were measured directly in the field. In addition, the variation in bed thickness along the folded layers was also measured. Bed-thickness variation along the folds' profile is a parameter typically used by structural geologists for the classification of folds, as it relates with the mechanisms and environmental conditions (pressure and temperature) that dominate during folding (Ramsey and Huber, 1987). If the outcrop and the bedding orientation are known, simple trigonometry will give true bed-thickness values; however, the accurate measurement of these parameters along the folded layers would require too much effort to be applied extensively in the field when the folds are hectometric (100 m) or larger in size, and/or the terrain is difficult to access. Therefore, geologists generally do not quantify thickness variations in the field; rather they tend to be qualitatively descriptive. An easier way to calculate the true thickness along folded layers is by the use of orthorectified images oriented perpendicular to the direction of the plunging fold axis, since folds should be observed on a section that is orthogonal to their axis direction.

3D Model of the Fold

The outcrop was photographed with a Canon EOS 450D digital single-lens reflex camera, having a 12.1 Mpixel sensor and EF-S 18 to 55 mm f/3.5 to 5.6 IS lens. A large number of photographs (351) were taken at various distances from the outcrop and at different focal lengths, and were used to build an extremely detailed (dense) model of the fold (Figs. 2 and 4). As seen in Fig. 2, photographs were taken from approximately three different sets of camera-to-object distances. Close-up photographs covered a photographed area of about 0.33 m × 0.22 m each (about 167 pixels/mm²). Photographs from the second set that were perpendicular to the outcrop portray an area of about 2.32 m × 1.55 m (3.4 pixels/mm²) (it is difficult to define the resolution of photographs that are at different (oblique) angles to the outcrop). Finally, perpendicular photographs from the furthest set have resolution of about 1.59 pixels/mm².

Screenshots from PhotoScan during model building are shown in Fig. 4. The dense point cloud contained 23 million points with a resolution of about 58 points per cm². Triangles comprising the mesh have an average area of about 1.8 mm² each). Differences between measurements in the field made by the laser distance meter and the digitally computed distances of targets are within about ±2 cm of each other (Fig. 5(a)), and are insensitive to the X, Y and Z coordinate directions (Fig. 5(b)).

Geological Data Extraction and Photo-realistic Cross Section

The textured model was exported from PhotoScan as Wavefront OBJ (.obj) and then imported into OpenPlot. In this software, the traces of the intersections between the outcrop topography and the chosen planar geological features (such as bedding and fractures) were

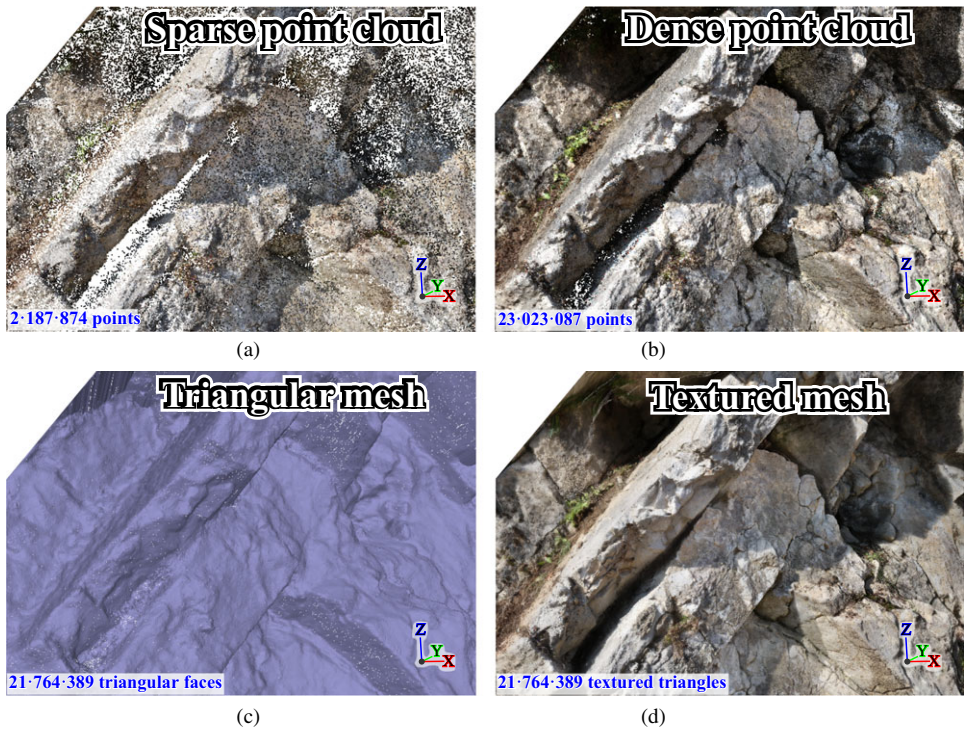


FIG. 4. Screenshots from PhotoScan showing: (a) the sparse point cloud after photo-alignment; (b) the point cloud after densification; (c) the triangular mesh derived from the dense point cloud; and (d) the textured mesh.

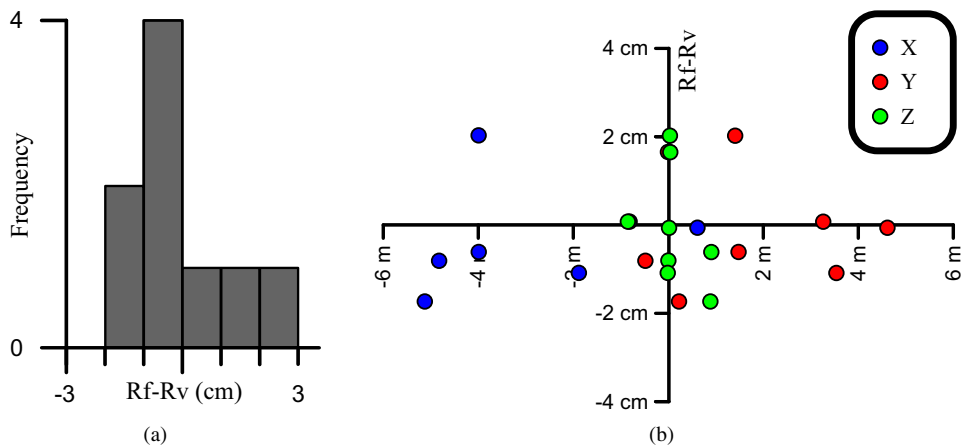


FIG. 5. (a) Histogram showing frequency of differences between measurements in the field made using a laser distance meter (R_f) and related distances in the virtual model (R_v). (b) Scatterplot with X, Y and Z coordinates on the abscissa and differences between R_f and R_v on the ordinate axis. The distribution of these differences is scattered and hence insensitive to the X, Y or Z coordinate directions.

manually digitised using point-by-point clicking. During the digitisation process, the moment of inertia of the picked points (which is based on the construction of a matrix of vectors that link each point to the centroid of the points) is computed (Fernández, 2005) and a best-fit plane for the digitised points is visualised in real time. This allows the user to evaluate and then accept or reject the resulting plane. This visual critical evaluation was very important in this workflow, since there are several possible sources of error (for example, local deformation of the model or collinearity of the digitised points; Fernández, 2005; Jones et al., 2016; Seers and Hodgetts, 2016b). In addition to this first qualitative method, the eigenvalues of the matrices resulting from the moment-of-inertia analysis (λ_1 , λ_2 and λ_3) were used to discard those planes resulting from highly collinear points. The degree of collinearity is defined by $K = \ln(\lambda_1/\lambda_2)/\ln(\lambda_2/\lambda_3)$ (Woodcock, 1977) so that planes having a degree of collinearity below 0.8 should be discarded (Fernández, 2005). However, due to the natural rugosity (wrinkling) of bedding surfaces, a case-by-case evaluation is preferred provided that the ratio between the maximum and middle eigenvalues is less than 30.

A total of 166 surface attitudes were measured using this approach (Fig. 6(a)). Of these, 65 were bedding surfaces and bed-parallel PSS and 101 were bed-perpendicular PSS, fractures and veins (Fig. 6(b)). The orientation of bedding surfaces and bed-parallel PSS fit to two maxima corresponding to planes dipping at $17^\circ/74^\circ$ (dip azimuth/plunge) and at

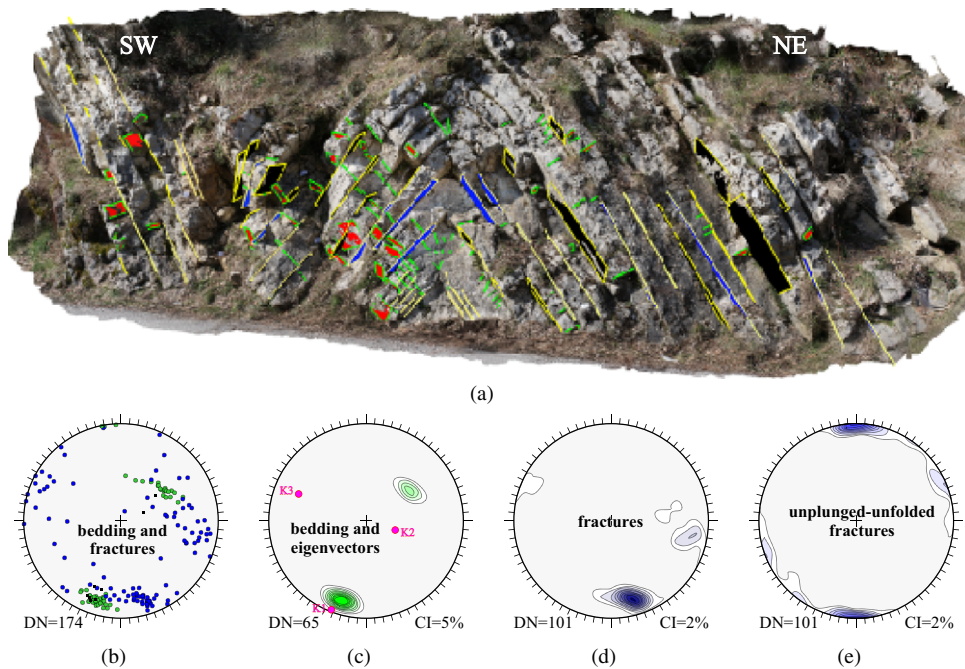


FIG. 6. (a) Screenshot of the model in OpenPlot with digitised structural elements (bedding, stylolites and joints). (b) Lower hemisphere, stereographic equal-area projections of poles to digitised bedding and bed-parallel PSS (green), to fractures (blue, both stylolites and joints) and to bedding measured in the field with a compass (black squares). (c) Contour plot of poles to bedding and results of tensorial analysis. (d) Contour plot of poles to fractures in their actual positions. (e) After fold plunge removal and unfolding. DN is the number of data points. CI is the contour interval.

234°/45° (Fig. 6(c)). Bed-perpendicular PSS and fractures form two major maxima corresponding to planes dipping at 273°/73° and 342°/74°, and a less representative one that corresponds to planes dipping at 115°/81° (Fig. 6(d)). A typical procedure used by structural geologists when dealing with fracture systems in folded layers is that of analysing fractures after bedding dip removal to unravel the timing relationships between folding and fracturing. For instance, after the removal of the plunge of the fold and the residual bedding dip, these bed-perpendicular features, are oriented E–W, N–S and NW–SE (Fig. 6(e)). The observed E–W and N–S structures are oblique to the general NW–SE trend of the fold, however, joints with these trends have been already described in the area (Marshak et al., 1982; Tavani et al., 2008).

To extract further quantitative information from the case study anticline, a cross section was produced. The cross section has to be oriented normal to the direction of the fold axis (the line of intersection of the fold limbs). In a stereoplot (such as those shown in Fig. 6), this can be estimated through a π -diagram (Ramsay and Huber, 1987; Fig. 7(b)) graphical method: if a fold is cylindrical (Fig. 7(a)), each pole to bedding is at an angle of 90° to the fold axis and each pole is ideally located on a great circle of the stereonet. The pole of a great circle passing through the poles to bedding of that fold is thus parallel to the fold axis (Ramsay and Huber, 1987; Fig. 7(b)). Solving this great circle in a graphical manner is complicated by the fact that poles to bedding generally do not lie perfectly on a unique great circle for several reasons (Ramsay and Huber, 1987). Given that, in a fold, the poles to bedding are distributed around a plane, the fold's axis can also be imagined as having the direction of least distribution of poles. From tensor analysis of poles to bedding and bed-parallel PSS, three mutually orthogonal eigenvectors with their relative eigenvalues were therefore derived (Whitaker and Engelder, 2005) (Fig. 6(c)). The smallest eigenvalue corresponds to the direction of minimum concentration of poles and hence to the direction of the intersection between the two limbs of the fold (the statistical direction of the fold axis).

In PhotoScan, the model was rotated to set the direction of the smallest eigenvector, 292°/26°, corresponding to the β axis of the fold, parallel to one of the principal axes. An orthomosaic (which is equivalent to a photo-realistic cross section) perpendicular to the direction of the fold axis was then produced (Fig. 8).

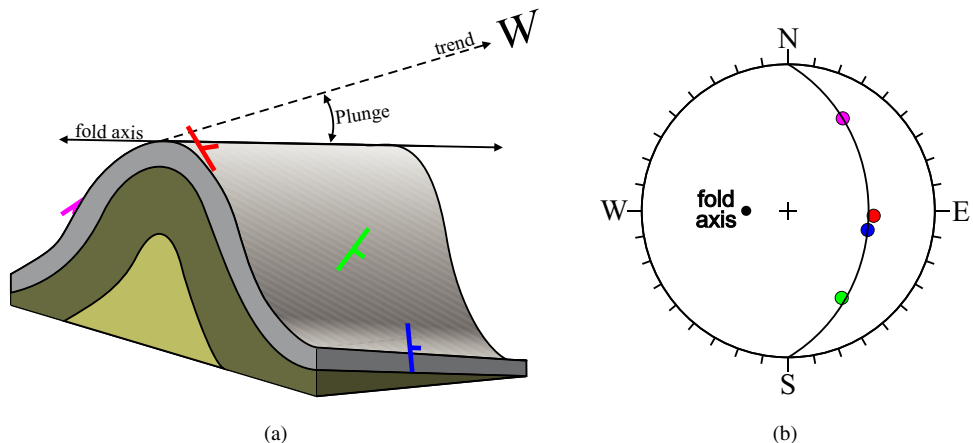


FIG. 7. (a) Scheme of a cylindrical plunging fold showing bedding dips with (b) relative stereoplot and relative interpolating great circle.



FIG. 8. Orthorectified image of the studied fold, oriented perpendicularly to the β axis.

Analysis of the Orthorectified Model

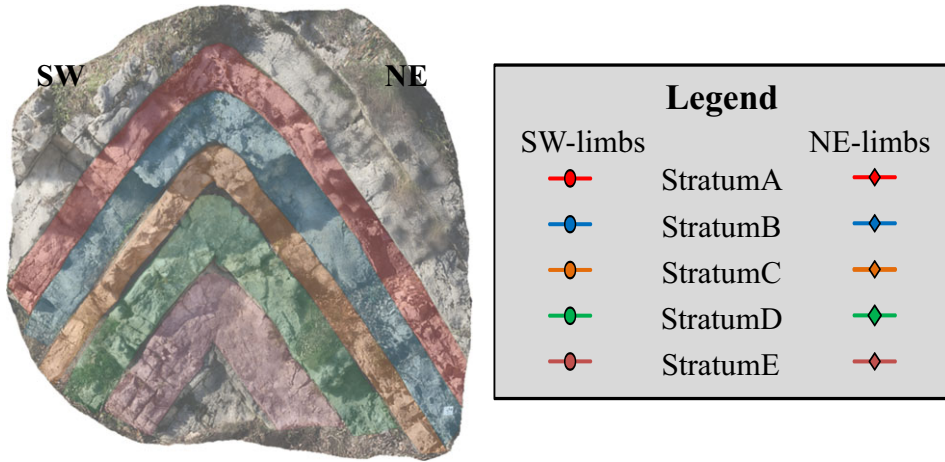
The fold, as observed in the cross section of Fig. 8, can be classified with two distinct superposed profiles. In fact, in the lower part, the fold is characterised by long planar limbs and a short angular hinge zone, while the hinge zone in the upper part presents a bulbous shape (Ramsay, 1974). The angle between the two limbs (the interlimb angle) is 72.2° , so the fold can be classified as an open fold (interlimb angle between 120° and 70°) according to its degree of tightness/openness (Twiss, 1988).

One of the most evident advantages of working on a properly oriented cross section is the possibility of deriving accurate stratimetry (that is, measurements of bed thicknesses) and hence, with respect to this study case, evaluating bed thickening/thinning along each stratum of the fold. The thickness of five strata (Fig. 9(a)) were measured from the orthorectified image, with a sampling step of 12 cm from their hinges (Fig. 9(b)). As was appreciated in the field in a preliminary qualitative manner, the thickness profiles of the strata in Fig. 9(b) show modest hinge thickening, whereas away from the hinge, strata decrease in thickness. This decrease is not constant, neither among strata nor between limbs of the same stratum.

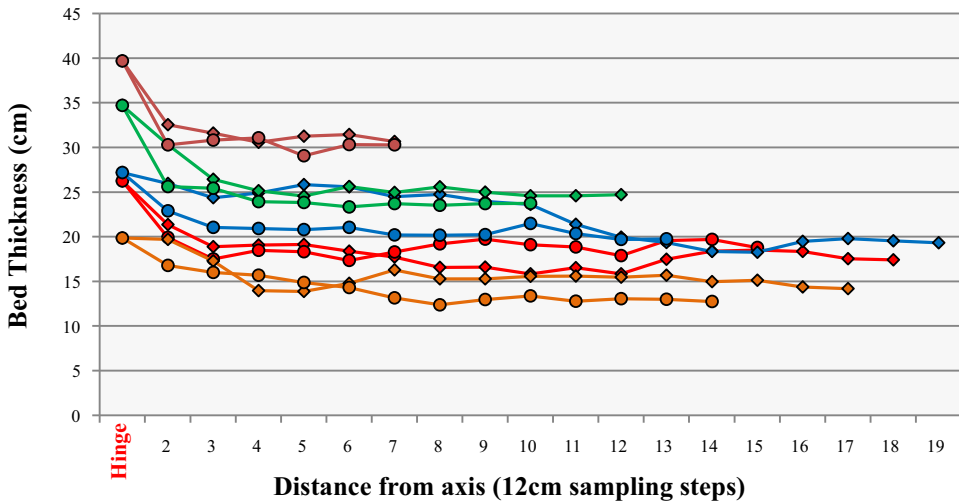
To understand if hinge thickening is proportional to bed thickness, the thickness of each bed has been normalised using the average thickness of each stratum (Fig. 10). No correlation between pristine bed thickness and the amount of hinge thickening has been found. Strata show thickness variations of about $\pm 10\%$ along the limbs and hinge thickening from about 28% to 47%, which is not proportional to bedding thickness.

DISCUSSION

In earth sciences, the quantitative analysis of geological structures, like folded layers, faults, thrust-related anticlines and fractures, relies on the availability of undistorted cross



(a)



(b)

FIG. 9. (a) Scheme highlighting the thickness of five strata. (b) Graph showing thickness variations of the coloured strata from the hinge outward with sampling steps of 12 cm.

sections of the target geological object. This is easily obtained at small scales as achieved, for example, with strain-marker analysis carried out with microphotographs (Fry, 1979). Similarly, 2D seismic lines integrated with techniques for geological cross-section construction has allowed the quantitative analysis of both the geometry and kinematics of fault-related folds (Suppe, 1983). In-between these micro- and macro-scales, there is a methodology void at the meso-scale. The quantitative analysis of geological structures occurring along exposures 1 to 100 metres wide is impeded by the unavailability of accurate and properly oriented cross sections. As an example, the analysis of fracture spacing carried out by means of scanlines (Korneva et al., 2014) requires orientation corrections

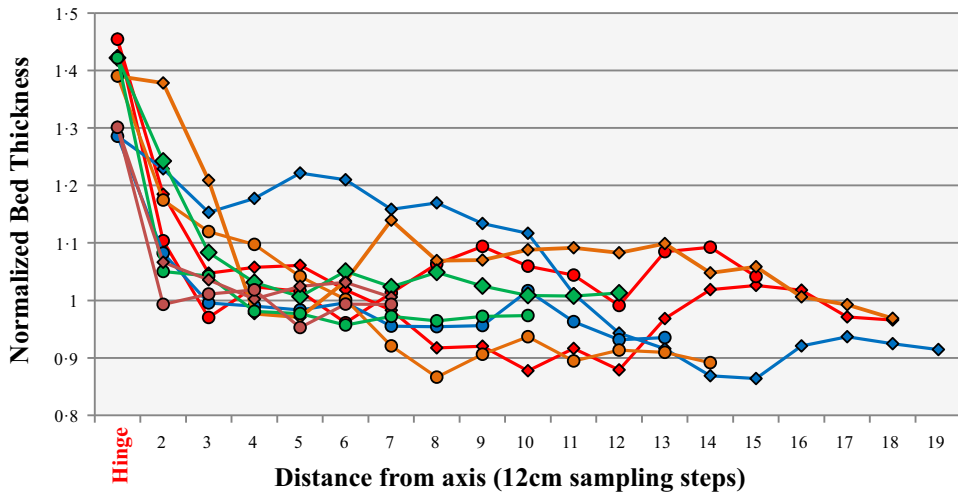


FIG. 10. Normalised bed thickness variations along the fold from hinge (left) to the limb. Sampling steps of 12 cm. The hinge thickening is about 25% to 47% of the mean thickness of the strata.

(Terzaghi, 1965), applied to input data that are, at best, affected by many centimetres of positioning errors. Similarly, the analysis of the shape of folds having wavelengths ranging between 1 and 100 metres is not possible, as this kind of analysis must be performed on properly oriented cross sections (Ramsay, 1974). This requires either: (1) a perfectly planar and fully accessible geological exposure, oriented perfectly perpendicularly to the fold axis; or (2) a high-resolution digital model of the outcrop. Indeed, the recent advent of lidar tools has allowed the quantitative analysis of structures ranging from one to several hundred metres. However, cost and portability issues with lidar equipment have prevented the application of 3D lidar models in the routine work of geologists. With digital photogrammetry, however, significant steps forward have been made. Nevertheless, the method still requires the use of bulky instrumentation for the accurate positioning of control points used to solve the registration of photogrammetrically derived 3D models. Since accurate registration of outcrops is often not necessary to field geologists, previous authors have tried to address the issue using less accurate but portable instrumentation (for example, Rieke-Zapp et al., 2009; Tavani et al., 2016). Here, a similar approach has been applied to the study of a plunging meso-scale fold affecting well-layered micritic limestones in the outer sector of the northern Apennines of Italy. A further case study that shows how geological issues can be addressed using photogrammetrically derived models and a few lightweight tools is of interest to many field geologists and geoscientists, working either in remote areas or interested in developing expertise in digital geology without the availability of huge budgets.

Users of such simple tools must in any case be aware that the potential sources of error are numerous. For instance, human error in positioning the devices or in reading of the measurements (plus the device's intrinsic error) can be significant and results must be validated, for example, by comparison with previous studies or direct field measurements. For this reason, in this study bedding attitudes collected from the model were compared with those measured in the field. Equal-area lower-hemisphere stereographic projections of poles to bedding from the model fall within those measured in the field (Fig. 6(b)).

In detail, mainly NE-dipping bedding attitudes were measured in the field, while just two bedding attitudes were measured in the SW-dipping part of the fold. One of these two is very close to the lower dipping zone of the fold hinge (Fig. 6(b)). Bedding attitudes from the model were instead measured from the flat and straight limbs of the folds (Fig. 6(a)), avoiding curved hinge zones. For this reason, field data are distributed along the direction perpendicular to the fold axis whereas model-derived bedding is clustered.

A good estimate of the fold axis was derived by tensor analysis of poles to bedding, which return three mutually orthogonal eigenvectors. The direction of the smallest eigenvector can be considered as the statistical direction of the fold axis (Fig. 6(c)). Therefore, the direction of this eigenvector was used to derive an orthomosaic of the fold (Fig. 8, which shows the fold profile). From this cross section, a series of bed-thickness measurements were easily taken.

This work also tried to obtain a proxy for the accuracy of the model by comparing measurements of distances made in the field using the laser distance meter with distances measured in the model. This is possible if one considers that the accuracy of the laser distance meter (1.5 mm, as stated by the manufacturer) is better than that associated with the low resolution of the graduated dial (1° for the azimuth). It was found that discrepancies in distances were within about ± 2 cm, and were insensitive to the *X*, *Y* and *Z* coordinate directions.

Even if this method cannot substitute a proper and robust analysis of the error (see, for example, Strecha et al., 2008), it allows verification that, broadly, no gross deformation exists away from the control points. Furthermore, bed-thickness measurements made from the cross section of the fold showed that hinge thickening is not related to the pristine thickness of the strata.

CONCLUSIONS

In this case study, the need for internal relative scales encouraged the authors to use less accurate but versatile instrumentation to obtain control points. This allowed the production of a geological cross section of a plunging meso-scale fold without noticeable deformation and therefore ready to extract quantitative information from it. Although the method was demonstrated in this work for the study of a fold, its potential is not limited to such formations. For instance, the method could be potentially decisive and provide a resolution for all cases where changing/heterogeneous stratigraphic/structural geometries are very difficult to assess, even in situ using direct contact with exposures. Examples include, but are not limited to, the study of:

- (1) Fan-shape syn-tectonic growth strata.
- (2) Inappreciable unconformities.
- (3) The slight thinning (due to bed-normal pressure solution) of carbonate beds associated with polygonal faults (Petracchini et al., 2015).
- (4) Deep-water outcrops using photo-realistic sections perpendicular to paleoflow (Arbués et al., 2012).

ACKNOWLEDGEMENTS

This is a contribution of: DiSTAR, University of Naples Federico II, Italy; Institut de Recerca Geomodels, University of Barcelona, Spain; Geodinàmica i Anàlisi de Conques

research group (2014SGR467SGR), Agència de Gestió d'Ajuts Universitaris i de Recerca (AGAUR), Spain; and Secretaria d'Universitats i Recerca del Departament d'Economia i Coneixement de la Generalitat de Catalunya, Spain. The final version of this paper benefited from the constructive reviews of Thomas D. Seers.

REFERENCES

- ARBÚÉS, P., GARCÍA-SELLÉS, D., GRANADO, P., LÓPEZ-BLANCO, M. and MUÑOZ, J. A., 2012. A method for producing photorealistic digital outcrop models. *74th EAGE Conference and Exhibition*, Copenhagen, Denmark. 5 pages. <https://doi.org/10.3997/2214-4609.20148218>
- BARCHI, M., LANDUZZI, A., MINELLI, G. and PIALLI, G., 2001. Outer Northern Apennines. In *Anatomy of an Orogen: the Apennines and Adjacent Mediterranean Basins* (Eds. F. Vai and I. P. Martini). Springer, Dordrecht, The Netherlands. 633 pages: 215–253.
- BARCHI, M. R., BROZZETTI, F. and LAVECCHIA, G., 1991. Analisi strutturale e geometrica dei bacini della media Valle del Tevere e della Valle Umbra. *Bollettino della Società Geologica Italiana*, 110(1): 65–76.
- BEAUDOIN, N., KOEHN, D., LACOMBE, O., LECOUTY, A., BILLI, A., AHARONOV, E. and PARLANGEAU, C., 2016. Fingerprinting stress: stylolite and calcite twinning paleopiezometry revealing the complexity of progressive stress patterns during folding – the case of the Monte Nero anticline in the Apennines, Italy. *Tectonics*, 35(7): 1687–1712.
- BEMIS, S. P., MICKLETHWAITE, S., TURNER, D., JAMES, M. R., AKCIZ, S., THIELE, S. T. and BANGASH, H. A., 2014. Ground-based and UAV-based photogrammetry: a multi-scale, high-resolution mapping tool for structural geology and paleoseismology. *Journal of Structural Geology*, 69(A): 163–178.
- BIGI, G., COSENTINO, D., PAROTTO, M., SARTORI, R. and SCANDONE, P., 1989. Structural model of Italy 1:500,000. Progetto Finalizzato Geodinamica. *Quaderni della Ricerca Scientifica CNR*, 114(3). 1 page.
- BISTACCHI, A., GRIFFITH, W. A., SMITH, S. A. F., DI TORO, G., JONES, R. and NIELSEN, S., 2011. Fault roughness at seismogenic depths from LIDAR and photogrammetric analysis. *Pure and Applied Geophysics*, 168(12): 2345–2363.
- BISTACCHI, A., BALSAMO, F., STORTI, F., MOZAFARI, M., SWENNEN, R., SOLUM, J., TUECKMANTEL, C. and TABERNER, C., 2015. Photogrammetric digital outcrop reconstruction, visualization with textured surfaces, and three-dimensional structural analysis and modeling: innovative methodologies applied to fault-related dolomitization (Vajont Limestone, Southern Alps, Italy). *Geosphere*, 11(6): 2031–2048.
- CORRADETTI, A., TAVANI, S., PARENTE, M., IANNACE, A., VINCI, F., PIRMEZ, C., TORRIERI, S., GIORGIONI, M., PIGNALOSA, A. and MAZZOLI, S., 2017. Distribution and arrest of vertical through-going joints in a seismic-scale carbonate platform exposure (Sorrento peninsula, Italy): insights from integrating field survey and digital outcrop model. *Journal of Structural Geology*, in press. <https://doi.org/10.1016/j.jsg.2017.09.009>
- ELTER, P., GIGLIA, G., TONGIORGI, M. and TREVISAN, L., 1975. Tensional and compressional areas in recent (Tortonian to present) evolution of the Northern Apennines. *Bollettino di Geofisica Teorica e Applicata*, 17: 3–18.
- FAVALLI, M., FORNACIAI, A., ISOLA, I., TARQUINI, S. and NANNIPIERI, L., 2012. Multiview 3D reconstruction in geosciences. *Computers & Geosciences*, 44: 168–176.
- FENG, Q., SJÖGREN, P., STEPHANSSON, O. and JING, L., 2001. Measuring fracture orientation at exposed rock faces by using a non-reflector total station. *Engineering Geology*, 59(1–2): 133–146.
- FERNÁNDEZ, O., 2005. Obtaining a best fitting plane through 3D georeferenced data. *Journal of Structural Geology*, 27(5): 855–858.
- FRY, N., 1979. Random point distributions and strain measurement in rocks. *Tectonophysics*, 60(1–2): 89–105.
- GRUEN, A., 2012. Development and status of image matching in photogrammetry. *Photogrammetric Record*, 27(137): 36–57.
- HODGETTS, D., 2013. Laser scanning and digital outcrop geology in the petroleum industry: a review. *Marine and Petroleum Geology*, 46: 335–354.
- JAMES, M. R. and ROBSON, S., 2012. Straightforward reconstruction of 3D surfaces and topography with a camera: accuracy and geoscience application. *Journal of Geophysical Research (Earth Surface)*, 117(F3). 17 pages. <https://doi.org/10.1029/2011jf002289>
- JAMES, M. R. and ROBSON, S., 2014. Mitigating systematic error in topographic models derived from UAV and ground-based image networks. *Earth Surface Processes and Landforms*, 39(10): 1413–1420.
- JONES, R. R., PEARCE, M. A., JACQUEMYN, C. and WATSON, F. E., 2016. Robust best-fit planes from geospatial data. *Geosphere*, 12(1): 196–202.

- KORNEVA, I., TONDI, E., AGOSTA, F., RUSTICHELLI, A., SPINA, V., BITONTE, R. and DI CUIA, R., 2014. Structural properties of fractured and faulted Cretaceous platform carbonates, Murge Plateau (southern Italy). *Marine and Petroleum Geology*, 57: 312–326.
- LOWE, D. G., 2004. Distinctive image features from scale-invariant keypoints. *International Journal of Computer Vision*, 60(2): 91–110.
- MARCHEGIANI, L., BERTOTTI, G., CELLO, G., DEIANA, G., MAZZOLI, S. and TONDI, E., 1999. Pre-orogenic tectonics in the Umbria–Marche sector of the Afro-Adriatic continental margin. *Tectonophysics*, 315(1–4): 123–143.
- MARSHAK, S., GEISER, P. A., ALVAREZ, W. and ENGELDER, T., 1982. Mesoscopic fault array of the northern Umbrian Apennine fold belt, Italy: geometry of conjugate shear by pressure-solution slip. *Geological Society of America Bulletin*, 93(10): 1013–1022.
- MASSIRONI, M., ZAMPIERI, D., SUPERCHI, L., BISTACCHI, A., RAVAGNAN, R., BERGAMO, A., GHIROTTI, M. and GENEVOIS, R., 2013. Geological structures of the Vajont landslide. *Italian Journal of Engineering Geology and Environment*, 2013(6): 573–582.
- MAZZOLI, S., DEIANA, G., GALDENZI, S. and CELLO, G., 2002. Miocene fault-controlled sedimentation and thrust propagation in the previously faulted external zones of the Umbria–Marche Apennines, Italy. *European Geosciences Union, Stephan Mueller Special Publication Series*, 1: 195–209.
- MCCAFFREY, K. J. W., FEELY, M., HENNESSY, R. and THOMPSON, J., 2008. Visualization of folding in marble outcrops, Connemara, western Ireland: an application of virtual outcrop technology. *Geosphere*, 4(3): 588–599.
- MOREELS, P. and PERONA, P., 2007. Evaluation of feature detectors and descriptors based on 3D objects. *International Journal of Computer Vision*, 73(3): 263–284.
- PEARCE, M. A., JONES, R. R., SMITH, S. A. F. and MCCAFFREY, K. J. W., 2011. Quantification of fold curvature and fracturing using terrestrial laser scanning. *AAPG Bulletin*, 95(5): 771–794.
- PETRACCHINI, L., ANTONELLINI, M., BILLI, A. and SCROCCA, D., 2015. Syn-thrusting polygonal normal faults exposed in the hinge of the Cingoli anticline, northern Apennines, Italy. *Frontiers in Earth Science*, 3 (November 2015): Article 67. 24 pages.
- PIERANTONI, P., DEIANA, G. and GALDENZI, S., 2013. Stratigraphic and structural features of the Sibillini Mountains (Umbria–Marche Apennines, Italy). *Italian Journal of Geoscience*, 132(3): 497–520.
- PLETS, G., VERHOEVEN, G., CHEREMISIN, D., PLETS, R., BOURGEOIS, J., STICHELBAUT, B., GHEYLE, W. and DE REU, J., 2012. The deteriorating preservation of the Altai rock art: assessing three-dimensional image-based modelling in rock art research and management. *Rock Art Research*, 29(2): 139–156.
- PRINGLE, J. K., CLARK, J. D., WESTERMAN, A. R., STANBROOK, D. A., GARDINER, A. R. and MORGAN, B. E. F., 2001. Virtual outcrops: 3-D reservoir analogues. *Journal of the Virtual Explorer*, 4(9): 51–55.
- RAMSAY, J. G., 1974. Development of chevron folds. *Geological Society of America Bulletin*, 85(11): 1741–1754.
- RAMSAY, J. G. and HUBER, M. I., 1987. *The Techniques of Modern Structural Geology: Folds and Fractures*. Academic Press, London, UK. 700 pages.
- REITMAN, N. G., BENNETT, S. E. K., GOLD, R. D., BRIGGS, R. W. and DUROSS, C. B., 2015. High-resolution trench photomosaics from image-based modeling: workflow and error analysis. *Bulletin of the Seismological Society of America*, 105(5): 2354–2366.
- REMONDINO, F. and EL-HAKIM, S., 2006. Image-based 3D modelling: a review. *Photogrammetric Record*, 21(115): 269–291.
- RIEKE-ZAPP, D. H., ROSENBAUER, R. and SCHLUNEGGER, F., 2009. A photogrammetric surveying method for field applications. *Photogrammetric Record*, 24(125): 5–22.
- SEERS, T. D. and HODGETTS, D., 2013. Comparison of digital outcrop and conventional data collection approaches for the characterization of naturally fractured reservoir analogues. *Geological Society Special Publication*, 374(1): 51–77.
- SEERS, T. D. and HODGETTS, D., 2016a. Extraction of three-dimensional fracture trace maps from calibrated image sequences. *Geosphere*, 12(4): 1323–1340.
- SEERS, T. D. and HODGETTS, D., 2016b. Probabilistic constraints on structural lineament best fit plane precision obtained through numerical analysis. *Journal of Structural Geology*, 82: 37–47.
- STRECHA, C., VON HANSEN, W., VAN GOOL, L., FUA, P. and THOENNESSEN, U., 2008. On benchmarking camera calibration and multi-view stereo for high resolution imagery. *IEEE Conference on Computer Vision and Pattern Recognition*. Pages 2838–2845.
- STURZENEGGER, M. and STEAD, D., 2009. Quantifying discontinuity orientation and persistence on high mountain rock slopes and large landslides using terrestrial remote sensing techniques. *Natural Hazards and Earth System Science*, 9(2): 267–287.
- SUPPE, J., 1983. Geometry and kinematics of fault-bend folding. *American Journal of Science*, 283(7): 684–721.

- TAVANI, S., STORTI, F., SALVINI, F. and TOSCANO, C., 2008. Stratigraphic versus structural control on the deformation pattern associated with the evolution of the Mt. Catria anticline, Italy. *Journal of Structural Geology*, 30(5): 664–681.
- TAVANI, S., ARBUÉS, P., SNIDERO, M., CARRERA, N. and MUÑOZ, J. A., 2011. Open Plot Project: an open-source toolkit for 3-D structural data analysis. *Solid Earth*, 2(1): 53–63.
- TAVANI, S., GRANADO, P., CORRADETTI, A., GIRUNDO, M., IANNACE, A., ARBUÉS, P., MUÑOZ, J. A. and MAZZOLI, S., 2014. Building a virtual outcrop, extracting geological information from it, and sharing the results in Google Earth via OpenPlot and Photoscan: an example from the Khaviz Anticline (Iran). *Computers & Geosciences*, 63: 44–53.
- TAVANI, S., CORRADETTI, A. and BILLI, A., 2016. High precision analysis of an embryonic extensional fault-related fold using 3D orthorectified virtual outcrops: the viewpoint importance in structural geology. *Journal of Structural Geology*, 86: 200–210.
- TERZAGHI, R. D., 1965. Sources of error in joint surveys. *Géotechnique*, 15(3): 287–304.
- THIELE, S. T., MICKLETHWAITE, S., BOURKE, P., VERRALL, M. and KOVESI, P., 2015. Insights into the mechanics of en-échelon sigmoidal vein formation using ultra-high resolution photogrammetry and computed tomography. *Journal of Structural Geology*, 77: 27–44.
- TWISS, R. J., 1988. Description and classification of folds in single surfaces. *Journal of Structural Geology*, 10(6): 607–623.
- ULLMAN, S., 1979. The interpretation of structure from motion. *Proceedings of the Royal Society of London. Series B Biological Sciences*, 203(1153): 405–426.
- VASUKI, Y., HOLDEN, E.-J., KOVESI, P. and MICKLETHWAITE, S., 2014. Semi-automatic mapping of geological structures using UAV-based photogrammetric data: an image analysis approach. *Computers & Geosciences*, 69: 22–32.
- VOLLGGER, S. A. and CRUDEN, A. R., 2016. Mapping folds and fractures in basement and cover rocks using UAV photogrammetry, Cape Liptrap and Cape Paterson, Victoria, Australia. *Journal of Structural Geology*, 85: 168–187.
- WACKROW, R. and CHANDLER, J. H., 2011. Minimising systematic error surfaces in digital elevation models using oblique convergent imagery. *Photogrammetric Record*, 26(133): 16–31.
- WHITAKER, A. E. and ENGELDER, T., 2005. Characterizing stress fields in the upper crust using joint orientation distributions. *Journal of Structural Geology*, 27(10): 1778–1787.
- WOODCOCK, N. H., 1977. Specification of fabric shapes using an eigenvalue method. *Geological Society of America Bulletin*, 88(9): 1231–1236.

Résumé

Un modèle 3D représentant un pli plongeant en chevron de taille moyenne dans le calcaire mésozoïque a été généré, mis à l'échelle et orienté en appliquant une chaîne de traitement basée sur la photogrammétrie. La mesure des strates a permis d'extraire le sens moyen de l'intersection entre les plans de strates (axe β du pli), permettant l'orthorectification du modèle 3D et la construction d'une section transversale photoréaliste. La méthode proposée constitue un outil novateur, disponible pour tous, pour une analyse quantitative précise des structures géologiques.

Zusammenfassung

Ein 3D-Modell einer abtauchenden, mittelgroßen Knickfalte in Kalkstein des Mesozoikums wurde in einem photogrammetrischen Arbeitsfluss generiert, mit Maßstab versehen und orientiert. Schichtmessungen erlaubten die Ableitung der statistischen Richtung des Schnitts zwischen Schichtebenen (die β -Achse der Falte) und die Orthorektifizierung des 3D-Modells und die Konstruktion eines photorealistischen Querschnitts. Dieser Beitrag stellt ein innovatives Werkzeug für Jedermann für die genaue, quantitative Analyse geologischer Strukturen bereit.

Resumen

En este trabajo se ha generado, escalado y orientado un modelo 3D de un anticlinal chevron de escala métrica integrando datos de buzamiento tomados en el campo con un flujo de trabajo basado en fotogrametría. Este flujo de trabajo permite primero, la ortorrectificación del modelo 3D usando el eje beta del anticlinal (es decir, la dirección estadística de intersección entre los dos flancos del pliegue), así como la posterior construcción de una sección geológica fotorealista carente de las distorsiones que impone la topografía del afloramiento. La metodología expuesta en este trabajo constituye una herramienta innovadora aplicable al análisis cuantitativo de estructuras geológicas.

摘要

本研究应用摄影测量的技术,生成一个中生代石灰岩的中尺度尖顶褶皱的三维模型,并对其进行尺度与方位的变换。层面的量测可以提取层面的交会方向(褶皱的 β 轴)之统计值,以进行三维模型的正射校正和生成具相片质感的横截面。本研究提出了一种可广泛应用于地质结构的精确定量分析的新工具。